COMPUTER METHODS IN MATERIALS SCIENCE

2024, vol. 24, no. 1, 15–24
https://doi.org/10.7494/cmms.2024.1.0832

Functionally graded porous material and its application in sandwich beams for bending and vibration behaviors

Lan Hoang Ton That

Faculty of Civil Engineering, HCMC University of Architecture, HCMC, Vietnam.

Abstract

The article describes a functionally graded porous material in an application for sandwich beams. The bending and vibration behaviors of this structure are studied using the finite element method based on a simple beam model. The influences of some parameters, e.g., the porosity factor or the exponent graded, are also studied in this article. Finally, the numerical results are presented with some discussion.

Keywords: functionally graded porous material, sandwich beam, bending, vibration, finite element method

1. Introduction

Nowadays, as a general perception, porous composites play an important role in the development of society. Their distinguishing feature is their interesting and varied geometries; for example, material distribution seems to have a lot of freedom in density control. The internal pores are closely related to changes in mechanical, electronic, thermal, biological, and chemical properties, making this material an attractive one for a range of applications. Some researchers consider porosity to be a manufacturing defect that can be graded and randomly dispersed whilst the porous structures discussed in other papers cover those specifically shaped for possible performance enhancement, reflecting the nature of such functionally graded materials.

There are two popular catalogues, as shown in Figure 1, to divide porous composites, i.e., by base material types and by geometrical features (Chen D. et al., 2023), where the former include ceramics, metals, concretes, polymers, and glasses, etc., (Ashby et al., 2000; Mei et al., 2021; Wu et al., 2021) while the latter relate to the distinguishable cellular morphologies with 3D regularised cells, 2D regularised cells, and stochastic open-/closed-cells (Chen E. et al., 2022; Shen et al., 2013; Veloso et al., 2022).

As shown in Mei et al., 2021, 3D porous ceramics have become a major research topic in recent years due to advantages such as their light weight and high durability, unlike traditional ceramic materials. By applying 3D printing techniques, hierarchical porous structures can be created by combining advanced manufacturing processes with flexible designs. This is considered a powerful and extremely attractive tool for making 3D porous ceramics. Nonlinear forced vibration of 2D functionally graded porous material beams were studied in (Wu et al., 2021). With bidirectional function, the material components gradient changed in both y and z directions of the beam. The vibration response curves are obtained by extracting the amplitude of the periodic motions based on the periodic response of the discrete system related to the pseudo-arc length technique.

Author's e-mail: tonthathoanglan.247@gmail.com
ORCID ID: 0000-0002-5195-1856

a)

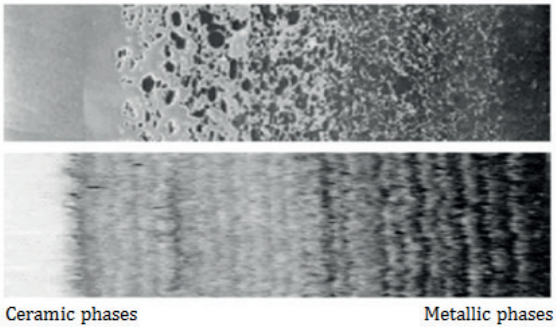

b)

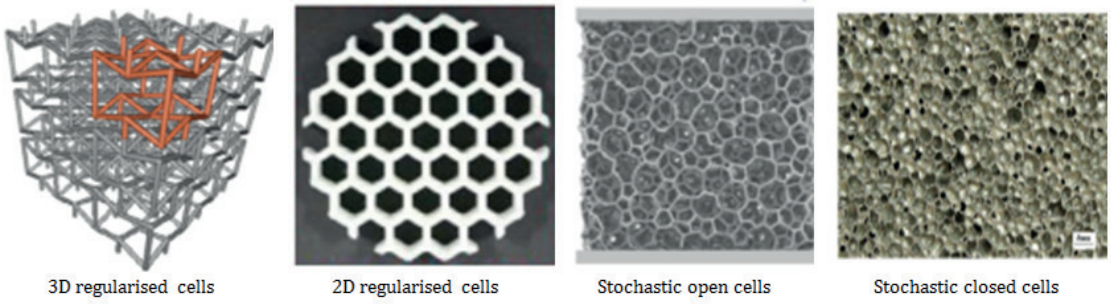

Fig. 1. Porous materials: a) classification by base materials; b) classification by geometrical features (Ashby et al., 2000; Chen E. et al., 2022; 2023; Mei et al., 2021; Shen et al., 2013; Veloso et al., 2022; Wu et al., 2021)

In another paper by Chen E. et al. (2022), using a function of key morphological features and the associated fracture properties of the parent solid to model the uniform and gradient densities, the authors estimated the strength of brittle open-cell foams. Moreover, to extract the Tessellation-based foam specimens with controlled microstructural characteristics corresponding to crushing strength, these authors suggested the high-fidelity numerical models that were used to reproduce the experimental data, and presented the complex relationship between foam microstructure and macroscopic failure. The paper of Shen et al. (2013) aimed to investigate the in-plane dynamic mechanical behavior of the functionally graded honeycomb. Finite element simulations were carried out using Abaqus/Explicit, woth interesting innovations discernible in both catalogues.

This article deals with the first type, especially for application in sandwich beams, which includes two different functionally graded face sheets and one homogenous ceramic core. This structure is widely applied in reality, such as in defense technology. For example, this structure with porosity can be used to reduce the weight of special military equipment, etc.

The bending and vibration behaviors of functionally graded porous sandwich beams using the simple finite element method are presented in this article as the main concern. The rest sections are established. The specific formulation for functionally graded porous sandwich beams, including the two cases of porosity, and for bending and vibration analyses are given in Sect. 2. The solutions to this study are presented in Sect. 3 and Sect. 4 supplies some necessary notes.

2. Formulations

A sandwich functionally graded porous (PFGS) beam of length L and thickness t is tested under uniform load q. This beam has two functionally graded face sheets and one homogenous ceramic core, as shown in Figure 2. Based on the appearance of porosity related to the porosity factor e in this structure, the study investigates two cases of porous distribution:

– case I with even porous face sheets,
– case II with a linear-uneven porous core.

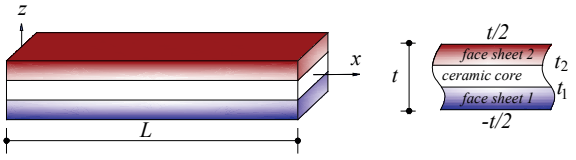

Fig. 2. Sandwich functionally graded porous beam

The values of material properties $P(z)$ are formulated in the Equations (1–2).

Case I

$$\begin{cases} P(z)=P_b+(P_c-P_b)\left(\dfrac{z+\dfrac{t}{2}}{t_1+\dfrac{t}{2}}\right)^n-(P_c+P_b)\dfrac{e}{2} & -\dfrac{t}{2}\le z\le t_1 \\ P(z)=P_c & t_1<z<t_2 \\ P(z)=P_t+(P_c-P_t)\left(\dfrac{z-\dfrac{t}{2}}{t_2-\dfrac{t}{2}}\right)^n-(P_c+P_b)\dfrac{e}{2} & t_2\le z\le\dfrac{t}{2} \end{cases} \tag{1}$$

Case II

$$\begin{cases} P(z)=P_b+(P_c-P_b)\left(\dfrac{z+\dfrac{t}{2}}{t_1+\dfrac{t}{2}}\right)^n & -\dfrac{t}{2}\le z\le t_1 \\ P(z)=P_c-eP_c\left(1-\dfrac{|2z-t_1-t_2|}{t_2-t_1}\right) & t_1<z<t_2 \\ P(z)=P_t+(P_c-P_t)\left(\dfrac{z-\dfrac{t}{2}}{t_2-\dfrac{t}{2}}\right)^n & t_2\le z\le\dfrac{t}{2} \end{cases} \tag{2}$$

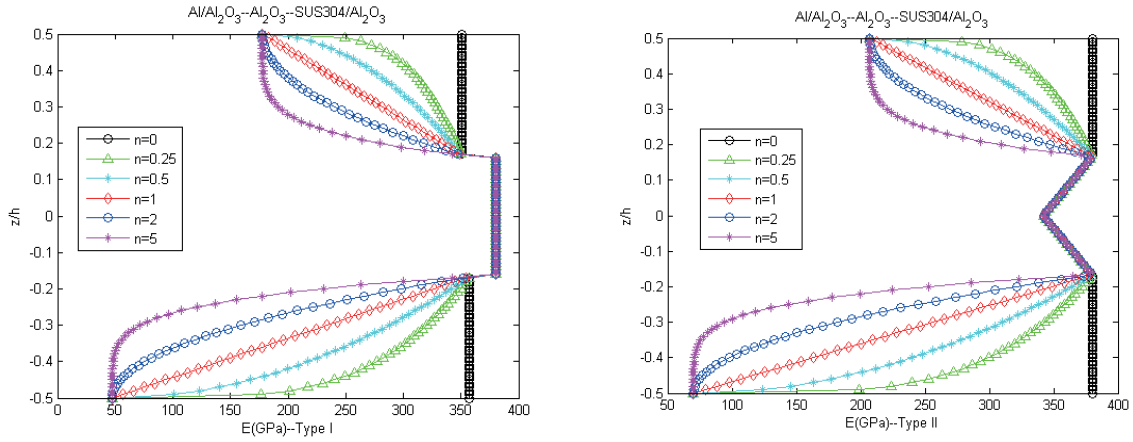

Fig. 3. The modification of E with $e = 0.1$, Al/Al_2O_3-Al_2O_3-SUS304/Al_2O_3 for Case I and II and the ratio of the thicknesses [1/1/1]

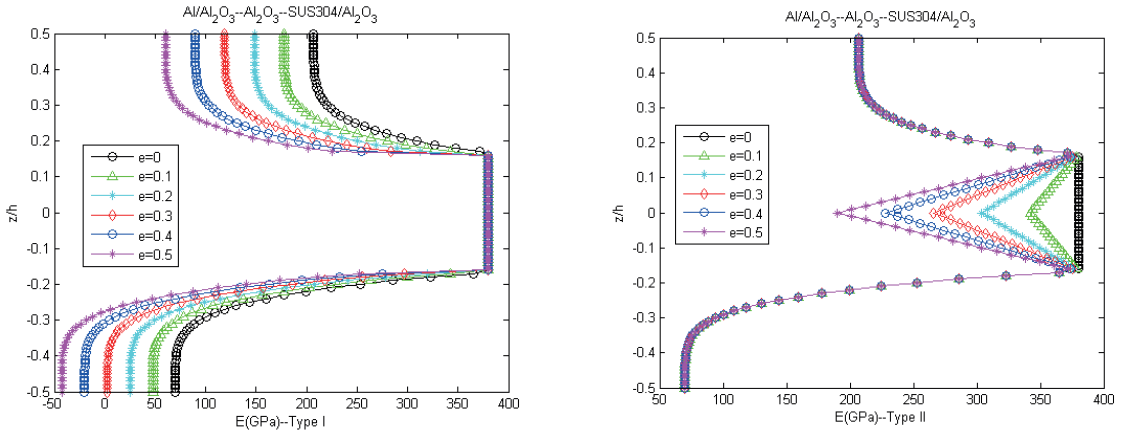

Fig. 4. The modification of E with $n = 5$, Al/Al_2O_3-Al_2O_3-SUS304/Al_2O_3 for Case I and II and the ratio of the thicknesses [1/1/1]

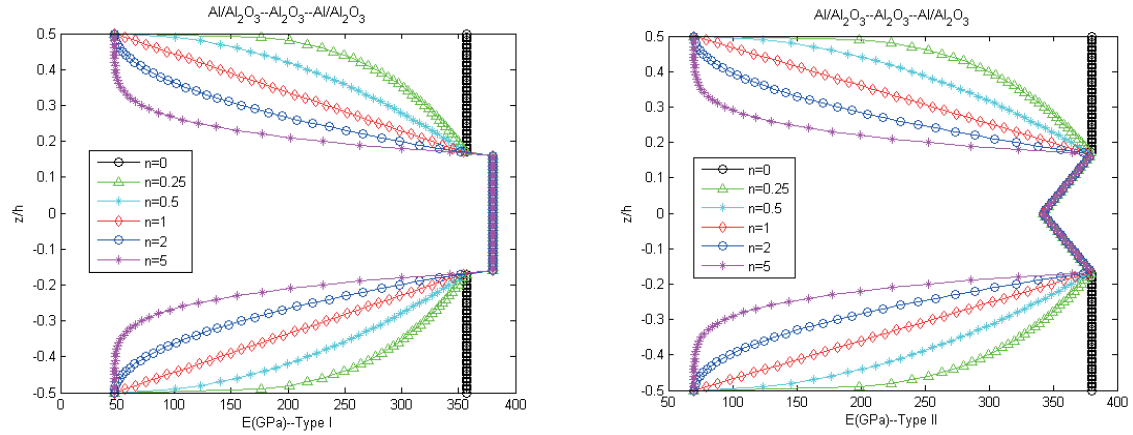

Fig. 5. The modification of E with $e = 0.1$, Al/Al_2O_3-Al_2O_3-Al/Al_2O_3 for Case I and II and the ratio of the thicknesses [1/1/1]

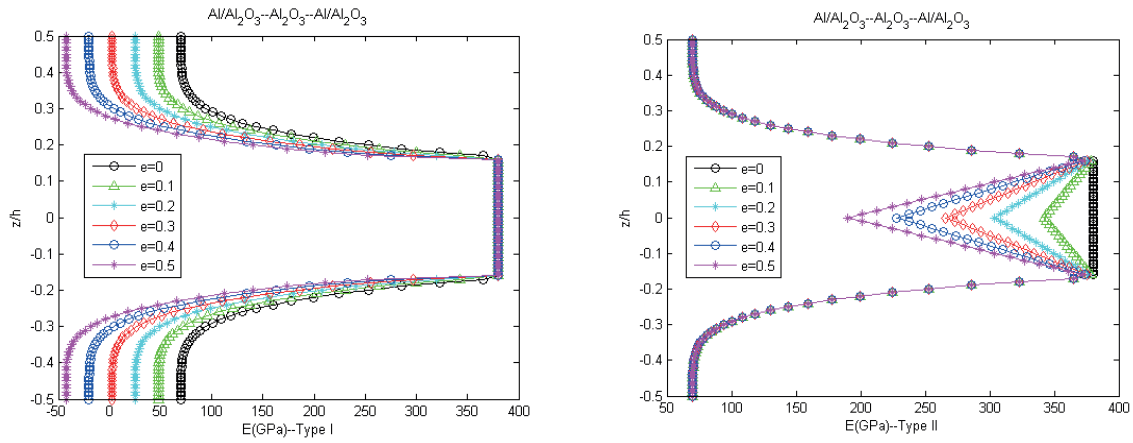

Fig. 6. The modification of E with $n = 5$, Al/Al_2O_3-Al_2O_3-Al/Al_2O_3 for Case I and II and the ratio of the thicknesses [1/1/1]

A group of three numbers like "$i_1 / i_2 / i_3$" is used to denote the ratio of the thicknesses of the bottom-core-top layers. That means the thickness of the bottom layer is $t.i_1 / (i_1 + i_2 + i_3)$, that of the core layer is $t.i_2 / (i_1 + i_2 + i_3)$ and that of the top layer is $t.i_3 / (i_1 + i_2 + i_3)$. The effective Young's modulus is demonstrated in Figures 3 and 4 with the beam containing one homogenous ceramic core of Al_2O_3, one bottom face sheet of Al/Al_2O_3 and one top face sheet of SUS304/Al_2O_3. Figures 5 and 6 also depict the modification of Young's modulus with a beam containing one homogenous ceramic core of Al_2O_3 and two face sheets of Al/Al_2O_3.

Based on the finite element procedure related to the simple beam model, the degrees of freedom associated with a node of an element are a deflection w and a rotation φ. The stiffness matrix of an element $\mathbf{K}_e$ can be written by (Felippa, 2004):

$$\mathbf{K}_e = \frac{E_e I_e}{L_e^3\left(1+\frac{12E_eI_e}{G_ekA_eL_e^2}\right)}\begin{bmatrix} 12 & 6L_e & -12 & 6L_e \\ 6L_e & \left(4+\frac{12E_eI_e}{G_ekA_eL_e^2}\right)L_e^2 & -6L_e & \left(2-\frac{12E_eI_e}{G_ekA_eL_e^2}\right)L_e^2 \\ -12 & -6L_e & 12 & -6L_e \\ 6L_e & \left(2-\frac{12E_eI_e}{G_ekA_eL_e^2}\right)L_e^2 & -6L_e & \left(4+\frac{12E_eI_e}{G_ekA_eL_e^2}\right)L_e^2 \end{bmatrix} + G_ekA_e\left(\frac{\frac{12E_eI_e}{G_ekA_eL_e^2}}{1+\frac{12E_eI_e}{G_ekA_eL_e^2}}\right)^2\begin{bmatrix} \frac{1}{L_e} & \frac{1}{2} & -\frac{1}{L_e} & \frac{1}{2} \\ \frac{1}{2} & \frac{L_e}{4} & -\frac{1}{2} & \frac{L_e}{4} \\ -\frac{1}{L_e} & -\frac{1}{2} & \frac{1}{L_e} & -\frac{1}{2} \\ \frac{1}{2} & \frac{L_e}{4} & -\frac{1}{2} & \frac{L_e}{4} \end{bmatrix} \quad (3)$$

where $k = 5/6$ is called the shear correct factor; E_e is the Young's modulus; I_e is the moment of inertia; L_e is the length of the element; G_e is the shear modulus, and A_e is cross-section area.

The element equation is given:

$$\mathbf{K}_e\mathbf{d}_e = \mathbf{F}_e \tag{4}$$

with

$$\mathbf{d}_e = \left[w_i \;\; \varphi_i \;\; w_j \;\; \varphi_j\right]^T, \mathbf{F}_e = \left[f_i \;\; m_i \;\; f_j \;\; m_j\right]^T \tag{5}$$

The mass matrix of an element can also be simplified by (Kien, 2007):

$$\mathbf{M}_e = \frac{1}{6}\rho L_e \begin{bmatrix} 2A_e & 0 & A_e & 0 \\ 0 & 2I_e & 0 & I_e \\ A_e & 0 & 2A_e & 0 \\ 0 & I_e & 0 & 2I_e \end{bmatrix} \tag{6}$$

with ρ is the mass density. After assembly, the deflections and frequencies can be obtained by solving the following equations:

$$\mathbf{Kd} = \mathbf{F} \tag{7}$$

$$\mathbf{M}\ddot{\mathbf{d}} + \mathbf{Kd} = \mathbf{0} \tag{8}$$

By using the three letters '*C*', '*S*' and '*F*' to refer to the clamped, simply supported and free condition, four kinds of boundary conditions can be taken as (SS), (CS), (CC) and (CF) for PFGS beams.

3. Numerical solutions of research

A (SS) sandwich functionally graded porous (PFGS) beam is considered under a uniform load *q*. The material properties of the beam are metal (Ti-6A1-4V) with E = 70 GPa, v = 0.3 and ceramic (ZrO_2) with E = 380 GPa, v = 0.3. The porosity factor *e* equals 0, for this example with case I. The deflection at position *L*/2 is normalized by $\bar{w} = 100E_m t^3 w(L/2)/q/L^4$. These values are compared with other results from other beam theories in (Belarbi et al., 2022; Sayyad, 2019) as shown in Table 1 or Figure 7 for only the ratio of the thicknesses [1/1/1].

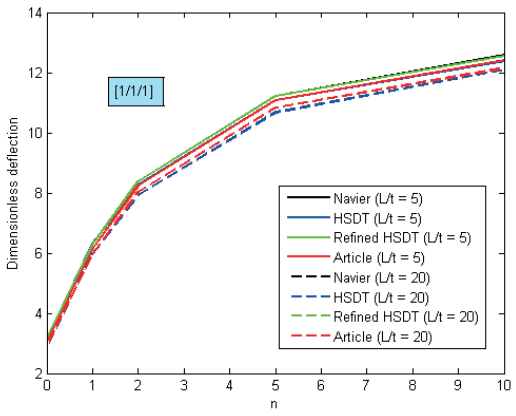

Fig. 7. The comparison of dimensionless deflections

Table 1. The comparison of the normalized deflections at position $x = L/2$ with $e = 0$ and case I

n	Model	*L*/*t* = 5		*L*/*t* = 20	
		[1/1/1]	[1/2/1]	[1/1/1]	[1/2/1]
0	Navier	3.1654	3.1654	2.8963	2.8963
	HSDT	3.1241	3.1241	2.8585	2.8585
	R-HSDT	3.1652	3.1652	2.8962	2.8962
	Present	3.0219	3.0219	2.8872	2.8872
1	Navier	6.2693	5.4122	5.9401	5.1006
	HSDT	6.3011	5.0341	5.9561	5.3415
	R-HSDT	6.2688	5.4125	5.9400	5.1006
	Present	6.1153	5.2602	5.9303	5.0910
2	Navier	8.3893	6.7579	8.0313	6.4276
	HSDT	8.2734	6.3359	7.9201	6.6697
	R-HSDT	8.3880	6.7581	8.0312	6.4276
	Present	8.2326	6.6028	8.0213	6.4178
5	Navier	11.2274	8.5137	10.8376	8.1642
	HSDT	11.0708	8.0576	10.6766	8.4045
	R-HSDT	11.2242	8.5134	10.8374	8.1642
	Present	11.0742	8.3584	10.8278	8.1543
10	Navier	12.5659	9.4050	12.1593	9.0471
	HSDT	12.3910	8.9290	12.1030	9.2824
	R-HSDT	12.5612	9.4041	12.1590	9.0470
	Present	12.4160	9.2514	12.1496	9.0373

In the paper of Belarbi et al. (2022), the authors conducted finite element analysis for beam structures, as stated in this article via a newly refined higher shear deformation theory. At the same time, in the study of Sayyad (2019), the authors presented Navier-type closed-form solutions for static bending, elastic buckling and free vibration analysis of symmetric functionally graded sandwich beams using a hyperbolic shear deformation theory. Based on the representation in Figure 7, it can be seen that the results obtained by the simple method, approximate their solutions quite well for both *L*/*t* ratios.

In order to clearly show the influence of material parameters as well as geometric characteristics on the deflection value, the modified code is done to achieve the results shown in Figures 8 and 9 and Tables 2 and 3. The increase of this deflection for the beam when increasing *n* and *e* is clearly different between case I and case II for both (CC) and (SS) boundary conditions, respectively.

By changing different boundary conditions as well as investigating the case of other thickness ratios, numerical results are obtained quite quickly with the largest deflection for the (CF) condition and obviously the smallest for the (CC) condition as shown in Table 4.

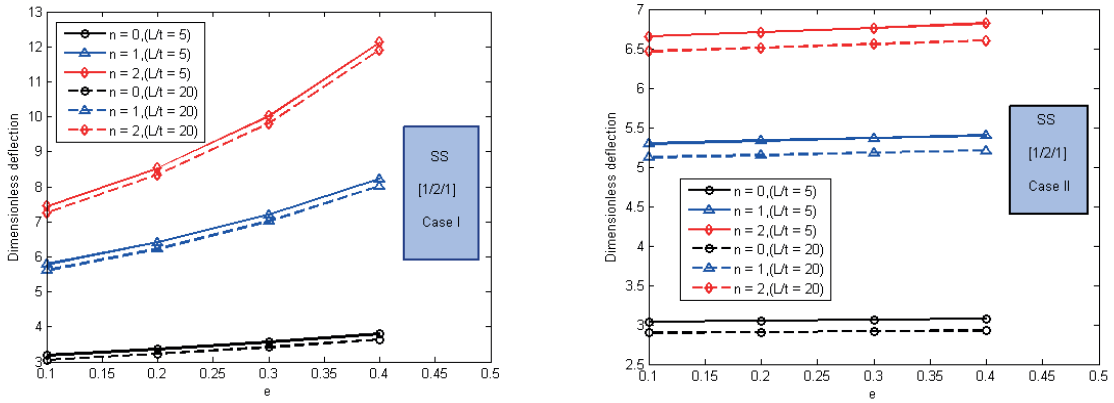

Fig. 8. The modification of dimensionless deflections with material: metal (Ti–6A1–4V) and ceramic (ZrO_2) for Case I and II and the ratio of the thicknesses [1/2/1] under (SS) condition

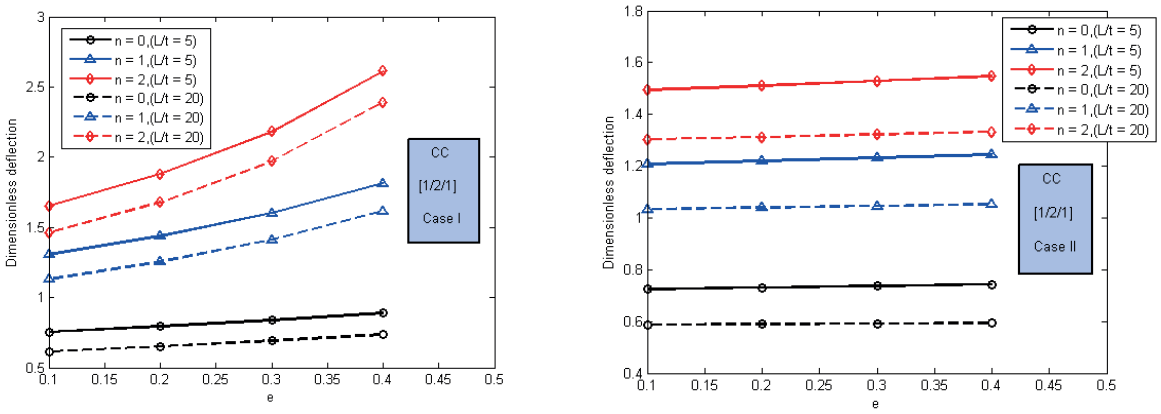

Fig. 9. The modification of dimensionless deflections with material: metal (Ti–6A1–4V) and ceramic (ZrO_2) for Case I and II and the ratio of the thicknesses [1/2/1] under (CC) condition

Table 2. The normalized deflections at position $x = L/2$ of (SS) beams

n	e	Case I			
		$L/t = 5$		$L/t = 20$	
		[1/1/1]	[1/2/1]	[1/1/1]	[1/2/1]
0	0.1	3.2018	3.1835	3.0616	3.0447
	0.2	3.4046	3.3636	3.2584	3.2204
	0.3	3.6351	3.5656	3.4823	3.4177
	0.4	3.8992	3.7936	3.7392	3.6408
1	0.1	6.9126	5.7785	6.7170	5.6027
	0.2	7.9520	6.4116	7.7445	6.2288
	0.3	9.3643	7.2031	9.1434	7.0127
	0.4	11.3959	8.2212	11.1596	8.0224
2	0.1	9.7571	7.4460	9.5319	7.2531
	0.2	11.9852	8.5401	11.7440	8.3387
	0.3	15.5542	10.0177	15.2946	9.8069
	0.4	22.2073	12.1243	21.9264	11.9033

n	e	Case II			
		$L/t = 5$		$L/t = 20$	
		[1/1/1]	[1/2/1]	[1/1/1]	[1/2/1]
0	0.1	3.0270	3.0346	2.8900	2.8964
	0.2	3.0322	3.0475	2.8928	2.9057
	0.3	3.0375	3.0608	2.8957	2.9151
	0.4	3.0428	3.0743	2.8985	2.9246
1	0.1	6.1312	5.2943	5.9419	5.1196
	0.2	6.1474	5.3290	5.9535	5.1484
	0.3	6.1639	5.3645	5.9652	5.1777
	0.4	6.1806	5.4008	5.9770	5.2072
2	0.1	8.2594	6.6547	8.0424	6.4631
	0.2	8.2865	6.7077	8.0636	6.5090
	0.3	8.3142	6.7620	8.0849	6.5557
	0.4	8.3423	6.8175	8.1063	6.6030

Table 3. The normalized deflections at position $x = L/2$ of (CC) beams

n	e	Case I			
		$L/t = 5$		$L/t = 20$	
		[1/1/1]	[1/2/1]	[1/1/1]	[1/2/1]
0	0.1	0.7600	0.7551	0.6198	0.6163
	0.2	0.8057	0.7949	0.6595	0.6517
	0.3	0.8574	0.8392	0.7046	0.6914
	0.4	0.9163	0.8891	0.7564	0.7363
1	0.1	1.5494	1.3056	1.3538	1.1299
	0.2	1.7674	1.4383	1.5599	1.2555
	0.3	2.0614	1.6031	1.8404	1.4127
	0.4	2.4807	1.8138	2.2445	1.6151
2	0.1	2.1436	1.6537	1.9183	1.4609
	0.2	2.6028	1.8798	2.3616	1.6785
	0.3	3.3323	2.1833	3.0727	1.9726
	0.4	4.6811	2.6134	4.4002	2.3924

n	e	Case II			
		$L/t = 5$		$L/t = 20$	
		[1/1/1]	[1/2/1]	[1/1/1]	[1/2/1]
0	0.1	0.7223	0.7248	0.5855	0.5866
	0.2	0.7253	0.7305	0.5860	0.5887
	0.3	0.7285	0.7364	0.5867	0.5908
	0.4	0.7317	0.7426	0.5874	0.5929
1	0.1	1.3878	1.2079	1.1985	1.0332
	0.2	1.3949	1.2199	1.2010	1.0393
	0.3	1.4023	1.2323	1.2036	1.0455
	0.4	1.4099	1.2453	1.2062	1.0517
2	0.1	1.8370	1.4944	1.6200	1.3028
	0.2	1.8476	1.5110	1.6246	1.3124
	0.3	1.8585	1.5284	1.6292	1.3221
	0.4	1.8698	1.5465	1.6338	1.3320

Table 4. The normalized maximum deflections $\bar{w} = \left(100E_m t^3 w_{\max}\right) / \left(qL^4\right)$ of PFGS beams under Cases I and II with $n = 1$ and $e = 0.1$

Case I	$L/t = 5$			
	SS	CC	CS	CF
[1/1/1]	6.9126	1.5494	3.0283	65.1927
[1/2/1]	5.7785	1.3056	2.5410	54.4235
[2/2/1]	6.1861	1.3969	2.7195	58.2692
[1/1/2]	7.0437	1.5856	3.0920	66.3810
Case II	$L/t = 5$			
	SS	CC	CS	CF
[1/1/1]	6.1312	1.3878	2.6983	57.7291
[1/2/1]	5.2943	1.2079	2.3387	49.7816
[2/2/1]	5.6325	1.2828	2.4861	52.9783
[1/1/2]	6.2747	1.4236	2.7645	59.0570
Case I	$L/t = 20$			
	SS	CC	CS	CF
[1/1/1]	6.7170	1.3538	2.8035	64.4102
[1/2/1]	5.6027	1.1299	2.3390	53.7205
[2/2/1]	5.9990	1.2098	2.5044	57.5206
[1/1/2]	6.8363	1.3783	2.8537	65.5517
Case II	$L/t = 20$			
	SS	CC	CS	CF
[1/1/1]	5.9419	1.1985	2.4808	56.9717
[1/2/1]	5.1196	1.0332	2.1380	49.0828
[2/2/1]	5.4493	1.0996	2.2756	52.2455
[1/1/2]	6.0771	1.2259	2.5374	58.2665

For free vibration analysis, the next verification of the proposed model is presented for PFGS beam. The material properties of the beam are assumed to be: metal (Al) with $E_m = 70$ GPa, $\nu_m = 0.3$, $\rho_m = 2{,}702$ kg/m^3 and ceramic (Al_2O_3) with $E_c = 380$ GPa, $\nu_c = 0.3$, $\rho_c = 3{,}960$ kg/m^3. The normalized natural frequency $\bar{\omega} = \left(\omega L^2 / t\right)\sqrt{\rho_m / E_m}$ is calculated for each case of the beam. By taking $e = 0$, $L/t = 20$ for Case I and changing n, these values are given in Table 5 and compared to other results in the paper by Vo et al. (2014).

Table 5. The normalized frequencies of (SS/CC) PFGS beams under Case I, $e = 0$ and $L/t = 20$

	BC	n	[1/1/1]	[1/2/1]	[2/2/1]
Vo et al.	SS	0	5.4603	5.4603	5.4603
Present			5.4692	5.4692	5.4692
Vo et al.		1	4.0328	4.2889	4.1602
Present			4.0362	4.2931	4.2017
Vo et al.		2	3.5389	3.8769	3.7049
Present			3.5412	3.8800	3.7807
Vo et al.	CC	0	12.2228	12.2228	12.2228
Present			12.3167	12.3167	12.3167
Vo et al.		1	9.0722	9.6411	9.3550
Present			9.1090	9.6860	9.4801
Vo et al.		2	7.9727	8.7262	8.3430
Present			7.9971	8.7592	8.5350

Finally, with two Cases I and II, $L/t = 5$ and 20, $e = 0.1$ and $n = 1$, the normalized frequencies of PFGS beams are given in Table 6 for several ratio thicknesses as well as four kinds of boundary conditions, respectively. Figure 10 also shows the first three mode shapes of PFGS beams with $e = 0.1$, $n = 1$ and $L/t = 20$.

Table 6. The normalized frequencies of PFGS beams under Cases I and II, $e = 0.1$ and $n = 1$

Case I	$L/t = 5$			
	SS	CC	CS	CF
[1/1/1]	3.8133	8.1516	5.7953	1.3789
[1/2/1]	4.0734	8.6733	6.1791	1.4738
[2/2/1]	3.9920	8.5025	6.0564	1.4444
[1/1/2]	3.8231	8.1552	5.8042	1.3831
Case II	$L/t = 5$			
	SS	CC	CS	CF
[1/1/1]	3.9540	8.4121	5.9953	1.4314
[1/2/1]	4.2111	8.9242	6.3732	1.5254
[2/2/1]	4.1079	8.7131	6.2197	1.4878
[1/1/2]	3.9288	8.3489	5.9538	1.4225

Case I	$L/t = 20$			
	SS	CC	CS	CF
[1/1/1]	3.9175	8.8436	6.1084	1.3970
[1/2/1]	4.1894	9.4544	6.5314	1.4940
[2/2/1]	4.1058	9.2660	6.4011	1.4642
[1/1/2]	3.9309	8.8722	6.1287	1.4018
Case II	$L/t = 20$			
	SS	CC	CS	CF
[1/1/1]	4.0704	9.1851	6.3456	1.4516
[1/2/1]	4.3404	9.7914	6.7656	1.5479
[2/2/1]	4.2328	9.5494	6.5982	1.5096
[1/1/2]	4.0458	9.1288	6.3070	1.4428

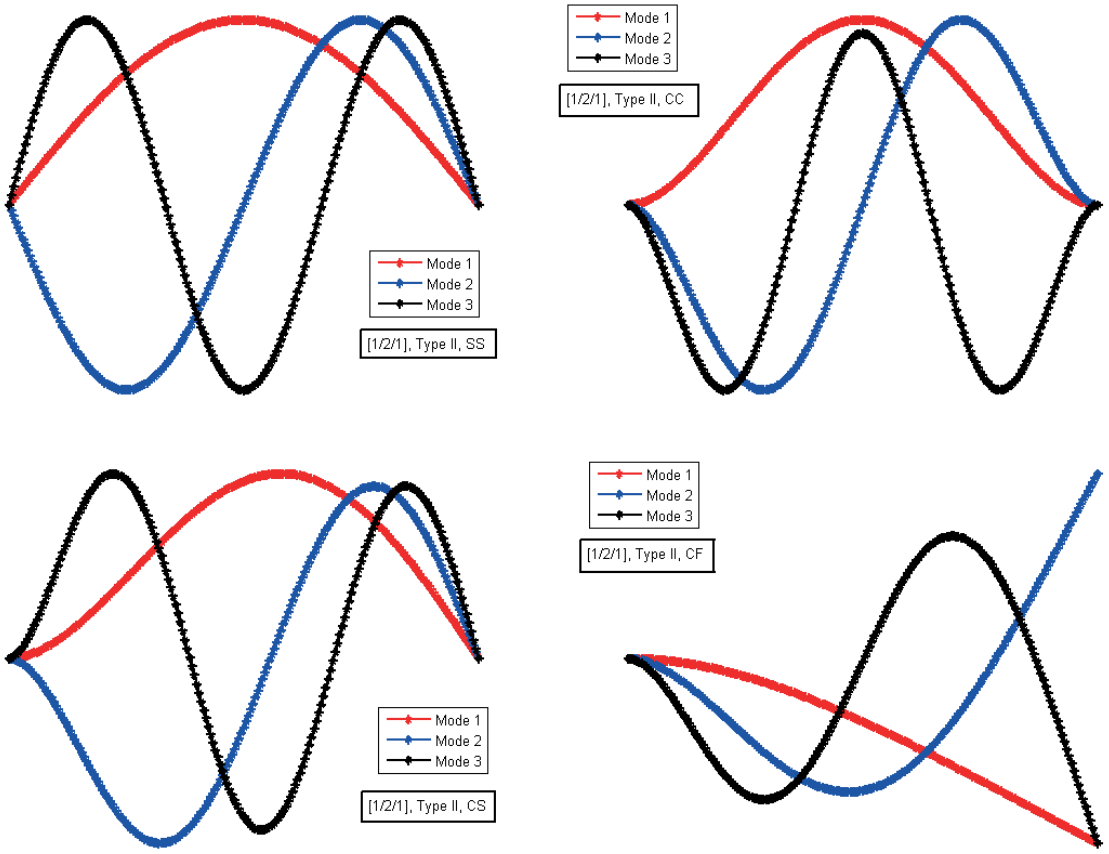

Fig. 10. The first three mode shapes of PFGS beams with $e = 0.1$, $n = 1$ and $L/t = 20$

4. Conclusions

The article presents the application of functionally graded porous material to sandwich beams. The bending and vibration behaviors of this beam are studied using the finite element method, based on a simple beam model. The influences of some parameters like n, e, L/t, ratio of thicknesses, or boundary conditions on numerical results are shown in this article. In case the engineer needs an overview of the bending and vibration behaviors of sandwich beams, this simple beam model can be used to quickly obtain results, a considerable advantage. However, in cases where engineers need more accurate results or deeper simulations of physical phenomena, they need to use more general theories or more accurate models which are lacking here.

References

Ashby, M. F., Evans, A. G., Fleck, N. A., Gibson, L. J., Hutchinson, J. W., & Wadley, H. N. G. (2000). *Metal Foams: A Design Guide*. Butterworth-Heinemann.

Belarbi, M.-O., Houari, M. S. A., Hirane, H., Daikh, A. A., & Bordas, S. P. A. (2022). On the finite element analysis of functionally graded sandwich curved beams via a new refined higher order shear deformation theory. *Composite Structures*, *279*, 114715. https://doi.org/10.1016/j.compstruct.2021.114715.

Chen, D., Gao, K., Yang, J., & Zhang, L. (2023). Functionally graded porous structures: Analyses, performances, and applications – A Review. *Thin-Walled Structures*, 191, 111046. https://doi.org/10.1016/j.tws.2023.111046.

Chen, E., Luan, S., & Gaitanaros, S. (2022). On the strength of brittle foams with uniform and gradient densities. *Extreme Mechanics Letters*, *51*, 101598. https://doi.org/10.1016/j.eml.2021.101598.

Felippa, C. A. (2004). *Introduction to Finite Element Methods*. https://quickfem.com/wp-content/uploads/IFEM.Ch00.pdf.

Kien, N. D. (2007). Free vibration of prestress Timoshenko beams resting on elastic foundation. *Vietnam Journal of Mechanics*, *29*(1), 1–12. https://doi.org/10.15625/0866-7136/29/1/5586.

Mei, H., Tan, Y., Huang, W., Chang, P., Fan, Y., & Cheng, L. (2021). Structure design influencing the mechanical performance of 3D printing porous ceramics. *Ceramics International*, *47*(6), 8389-8397. https://doi.org/10.1016/j.ceramint.2020.11.203.

Sayyad, A. S., & Avhad, P. V. (2019). On static bending, elastic buckling and free vibration analysis of symmetric functionally graded sandwich beams. *Journal of Solid Mechanics*, *11*(1), 166–180. https://doi.org/10.22034/jsm.2019.664227.

Shen, C. J., Lu, G., & Yu, T. X. (2013). Dynamic behavior of graded honeycombs – A finite element study. *Composite Structures*, *98*, 282–293. https://doi.org/10.1016/j.compstruct.2012.11.002.

Veloso, F., Gomes-Fonseca, J., Morais, P., Correia-Pinto, J., Pinho, A. C. M., & Vilaça, J. L. (2022). Overview of methods and software for the design of functionally graded lattice structures. *Advanced Engineering Materials*, *24*(1), 2200483. https://doi.org/10.1002/adem.202200483.

Vo, P. T., Thai, H.-T., Nguyen, T.-K., Maheri, A., & Lee, J. (2014). Finite element model for vibration and buckling of functionally graded sandwich beams based on a refined shear deformation theory. *Engineering Structures*, *64*, 12–22. https://doi.org/10.1016/j.engstruct.2014.01.029.

Wu, J., Chen, L., Wu, R., & Chen, X. (2021). Nonlinear Forced Vibration of Bidirectional Functionally Graded Porous Material Beam. *Shock and Vibration*, *2021*(1), 6675125. https://doi.org/10.1155/2021/6675125.